

Lawrence Berkeley National Laboratory

Recent Work

Title

Development of a Unique Laboratory Scale Fluidized Bed Wear Testing Unit

Permalink

<https://escholarship.org/uc/item/8jz7k8gj>

Authors

MacAdam, S.
Stringer, J.

Publication Date

1989-04-01



Lawrence Berkeley Laboratory

UNIVERSITY OF CALIFORNIA

Materials & Chemical Sciences Division

Presented at the Conference on Wear of Materials — 1989,
Denver, CO, April 9–13, 1989, and
to be published in *Wear*

Development of a Unique Laboratory Scale Fluidized Bed Wear Testing Unit

S. MacAdam and J. Stringer

April 1989

TWO-WEEK LOAN COPY

*This is a Library Circulating Copy
which may be borrowed for two weeks.*



DISCLAIMER

This document was prepared as an account of work sponsored by the United States Government. While this document is believed to contain correct information, neither the United States Government nor any agency thereof, nor the Regents of the University of California, nor any of their employees, makes any warranty, express or implied, or assumes any legal responsibility for the accuracy, completeness, or usefulness of any information, apparatus, product, or process disclosed, or represents that its use would not infringe privately owned rights. Reference herein to any specific commercial product, process, or service by its trade name, trademark, manufacturer, or otherwise, does not necessarily constitute or imply its endorsement, recommendation, or favoring by the United States Government or any agency thereof, or the Regents of the University of California. The views and opinions of authors expressed herein do not necessarily state or reflect those of the United States Government or any agency thereof or the Regents of the University of California.

LBL-28017

Development of a Unique Laboratory Scale
Fluidized Bed Wear Testing Unit

S. MacAdam
Lawrence Berkeley Laboratory
University of California
Berkeley, CA 94720

and

J. Stringer
Electric Power Research Institute
Palo Alto, CA

April 1989

This work was supported by the Electric Power Research Institute
under Research Project RP8000-6, through U.S. Department of
Energy Contract No. DE-AC03-76SF00098.

AUTHOR	<input checked="" type="checkbox"/>	EDITOR		MASTERCOPY	20 pages	WEA	5497
QUERIES	<input checked="" type="checkbox"/>	CORRECTION		Vol.	No.	pp.	

Only typographical correction will be accepted at this stage.

Wear, 00 (1989) 000 - 000

To be published in next issue.
Please send corrections
by return of mail.

DEVELOPMENT OF A UNIQUE LABORATORY SCALE FLUIDIZED BED WEAR TESTING UNIT*

STUART MACADAM

Lawrence Berkeley Laboratory, University of California, Berkeley, CA (U.S.A.)

JOHN STRINGER

Electric Power Research Institute, Palo Alto, CA (U.S.A.)

Summary

Significant wastage of internal bed components in fluidized bed combustors has been widely experienced throughout the industry. A major probable contribution to heat exchanger tube wastage in bubbling fluidized beds is mechanical in nature. It arises from the impact of blocks of defluidized particles thrown against tube undersides during either the passage of rising bubbles or the collapse of 'teardrop' like voids that form periodically under tubes. In an effort to investigate this process, isolated from other erosive or corrosive effects, a novel wear testing rig has been designed and built. This device simulates the particle block impact environment by the fast movement of a specimen rod vertically within a minimally fluidized bed. Data from initial room temperature tests indicate that rods exposed in the rig suffered losses which were similar in both magnitude and circumferential distribution to those experienced by tubes in other cold model studies that utilized more conventional fluidized bed units. The worn surface regions of the tested metallic rods were composed of a relatively hard multilayered composite of bed material and base metal that resulted from deposition of fine particle fragments and considerable surface deformation. Removal of material from this composite probably occurred primarily through a process of three-body microabrasion. For pure aluminum, a secondary process of layer spallation was active at circumferential locations where an exceptionally thick composite layer developed.

1. Introduction

Energy production from the fluidized bed combustion of coal has many advantages over conventional coal burning methods. A large reduction in emission of the pollutants NO_x and SO_x , as well as a high combustion efficiency and wide fuel tolerance, make fluidized bed combustion an attractive technology. A major problem encountered in the burning of coal by this process has been the material wastage of heat exchanger tubes and other

components immersed in the fluidized bed. This wastage involves mechanical wear processes combined in some instances with corrosion. Operation of fluidized bed combustors (fbc) has resulted in widely ranging tube wastage rates varying from essentially none, to unacceptable levels of 1000 nm h^{-1} or more [1]. This range suggests that wastage is not intrinsic to the fbc environment, but arises from design and operational characteristics.

1.1. Background

When an evenly distributed flow of gas passes upwards through a bed of solid particles at very low velocities, the particles remain stationary in the form of a packed bed, while the gas flows through interstices. If the flow is increased, the upward gas velocity (superficial velocity u_s) becomes sufficient to levitate the bed material. The bed is then said to be fluidized, and the air velocity at which this occurs is known as the minimum fluidizing velocity u_{mf} . The minimum fluidizing velocity is dependent on the gas density, particle density, and particle size. As the flow is increased, the bed expands and becomes less dense as inter-particle spacing increases. At some point, increased gas flow results in instabilities within the bed leading to the creation of bubbles near the distributor that grow by coalescence and rise through the bed. In most fbc systems, where the coal and sorbent particles are larger than $400 \mu\text{m}$, this instability exists immediately upon fluidization so that the minimum bubbling velocity u_{mb} is equal to u_{mf} . Within the bubbling regime, increasing η_s leads to a more violent bubbling and resultant large pressure fluctuations until a transition into the turbulent fluidization regime occurs. In the turbulent regime, small voids form and disappear throughout the bed in a random manner; pressure fluctuations are correspondingly small. The majority of fbc operate under a bubbling regime.

1.2. Particle block hammering process

Mechanical wear in bubbling fluidized beds may result from many causes; some may be intrinsic to certain regimes in the fluidized bed environment while other are related to design or operational aspects. These processes, which have been discussed by Stringer and Wright [2], include both high velocity, dilute phase erosive conditions, and high particle loading, dense phase abrasive conditions. One process which may be a major intrinsic contributor to the wastage of horizontal heat exchanger tubes immersed in bubbling beds arises from the impact of blocks of essentially defluidized particles on the underside of tubes. Experiments with cameras situated inside clear tubes have shown such particle blocks hammering tube bottoms with great force, and then dropping away or sliding upward across their surfaces [3]. External viewing through clear bed walls has indicated that these impacts are associated both with the wakes of rising bubbles and the collapse of 'teardrop' like voids that form periodically beneath tubes [4]. Rising bubbles and the resulting particle blocks typically have a velocity of between 1 and 3 Hz. Peak forces on tubes associated with these block impacts have been measured to be in the range 50 - 800 N [5] depending on bed dimensions and fluidizing characteristics.

The experimental evidence thus suggests that instead of individual bed particles freely striking the tubes, a particle is constrained to be in sliding contact with the tube for some time, loaded onto the surface by the block of unfluidized particles of which it is a member. This implies an abrasive wear process, rather than an erosive process. The particles appear to have some limited ability to move and rotate relative to one another and to the tube surface, which is consistent with a three-body abrasive process. Actually, it may well be that the true wear process includes aspects of both erosion and abrasion; more detailed analysis of the wear process is beyond the scope of this paper. The aim of this research is to study that part of the tube wear associated with the impact of blocks of particles, either in the wakes of bubbles or resulting from the collapse of teardrop voids.

1.3. Actuated specimen rig

In an effort to investigate this process, isolated from other effects, and in a controlled environment, a small fluidized bed unit has been designed and built with the unique feature of a horizontal specimen rod that can be quickly moved a short distance vertically within a minimally fluidized bed. The downward specimen motion is controlled to produce similar frequencies and velocities as those of the impacting particle blocks observed in bubbling fluidized beds. The resulting measured impact force is also similar to that which has been measured in real systems. Since the bed is minimally fluidized during testing, all other contributions to wear are essentially eliminated.

The actuated specimen test rig overcomes problems associated with conventional fluidized bed wastage testing units involving high cost and limited control. To recreate the environment typical of bubbling fbc, a fluidized bed wear testing unit would need to be rather large ($>0.6 \text{ m} \times 0.6 \text{ m}$) so as to overcome wall effects and to allow small bubbles the opportunity to coalesce into potentially more damaging larger ones. The maximum available fluidizing velocity would need to be as high as 2 m s^{-1} . In such a large unit, control of temperature and local fluidizing behavior is difficult. Moreover, these conditions would require a large capacity air blower, capable of $1 \text{ m}^3 \text{ s}^{-1}$, and some means of introducing around 250 kW in order to achieve fbc temperatures of $600 \text{ }^\circ\text{C}$. Since the laboratory rig relies on specimen motion to simulate interactions with bubbles or teardrop voids, it can be operated at u_{mf} , essentially eliminating the effects of wall proximity and long-range flow patterns. The rig is thus scaled to accommodate the selected specimen size and to assure realistic fluidizing conditions. The required flow rate for the rig is $0.015 \text{ m}^3 \text{ s}^{-1}$. A 4 kW external furnace is all that is necessary to heat this unit, making it possible to determine the temperature dependence of the wastage. In this paper, two tasks designed to qualify the rig cold by comparison with tests in large cold model fluidized beds are described. Investigations at elevated temperature will be presented elsewhere.

2. Experimental apparatus

A schematic of the fluidized bed wear testing rig is shown in Fig. 1. Dimensions and other characteristics are listed in Table 1. The body of the unit consists of a 155 mm diameter enclosed vertical cylinder that is partially filled with bed material. Quartz with a mean particle diameter of $800\ \mu\text{m}$ was the material chosen in this study because it is often a major constituent of the inert bed material within fbc, and is believed to be primarily responsible for component wear. Air is fed to a distributor within the bed consisting of four tubes extending radially from a central supply tube. Each tube extension has two holes on its underside. When in operation, air enters the bed via the eight distributor holes, flowing first downward and then uniformly upward through the bed towards the exhaust at the top, where it passes through a cyclone that collects escaping particle dust. The bed material, a few centimeters below the distributor, is not penetrated

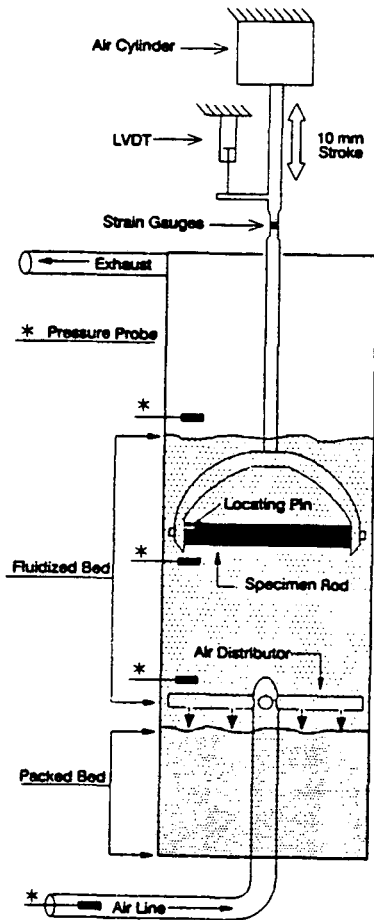


Fig. 1. Schematic diagram of actuated specimen fluidized bed wear testing rig.

TABLE 1

Fluidized bed characteristics and ranges of operating conditions

<i>Fluidized bed dimensions</i>	
Bed diameter	155 mm
Bed depth range	102 - 914 mm
Specimen dimensions	108 mm long x 19 mm diameter
<i>Ranges for fluidizing and actuation characteristics</i>	
Number of holes	8
Hole diameter	4 at 4.0 mm, 4 at 4.4 mm
Pressure drop	6.9 kPa (1 psi) at 0.50 m s^{-1}
<i>Distributor characteristics</i>	
Fluidizing velocity	$0.25 - 1.25 \text{ m s}^{-1}$
Maximum specimen velocity	$0.8 - 2.0 \text{ m s}^{-1}$
Specimen actuation frequency	0.27 - 2.8 Hz
Specimen actuation amplitude	0 - 20 mm full deflection

by the air jets and thus remains in the packed condition. Typical distributors sit at the bottom of the bed and have orifices directed upward. The downward directed orifices of this rig prevent jet streaming, and thus allow the specimen to be situated close to the distributor. This design also helps prevent orifice blockage which can result in preferential bubble paths and uneven fluidization. By adjusting the height of the distributor, the bed depth can be altered.

The specimen is a rod of circular cross-section, held horizontally in a stirrup on the end of an actuator rod within the fluidized portion of the bed. Specimen orientation is maintained with a locating pin. The specimen rod is driven downward within the fluidized bed at high accelerations by a pneumatic air cylinder. The force of the downward stroke is altered by adjusting the air pressure supplying the cylinder. The bed material immediately below the moving specimen is compressed, or defluidized, and therefore behaves like the defluidized material that is thrown against the tube bottom during bubble passage or teardrop void collapse in bubbling fbc. The specimen accelerates at an approximately constant rate from its rest position at the top of the stroke to the stroke end. Typical values for this acceleration range $60 - 170 \text{ m s}^{-2}$. The characteristics of the downward specimen motion were modeled after those of rising bubbles and collapsing teardrop voids. Maximum downward specimen velocities, like those of rising bubbles, are in the range $1 - 2 \text{ m s}^{-1}$. The actuation frequency can be set between 0.27 and 2.8 Hz, similar to the measured pressure and tube force pulses of 0.5 - 3 Hz. The stroke length can be set between 0 and 20 mm. This is in the range of the observed teardrop dimensions of 10 - 50 mm. The return stroke is damped to prevent any significant wear occurring during the upward stroke since the system is meant to simulate particle blocks that impact the tube bottom only. The downward specimen motion typically takes between

10 and 15 ms for a 10 mm stroke. The specimen spends the remainder of the cycle time stationary at the ends of the stroke, or being slowly drawn to the top of the stroke.

Specimen motion is monitored through a linear variable displacement transducer (LVDT) attached to the actuating rod. The force of particle blocks impacting the rod surface is determined via strain gauges that are mounted on a reduced section of the actuating rod. Pressure transducers are linked to probes that can be inserted into the bed through side ports located at intervals along the tube. These probes are used to determine the onset of fluidization and to detect any bubbling that occurs within the bed.

3. Operational characterization

3.1. Bed particle conditioning

During the first several hours of fluidized bed operation with fresh bed material, nearly 20% of the quartz was reduced to fines and elutriated. This was found to be due more to the rounding of particles by the cracking off of corners than to bulk fragmentation. After this initial period, the particles reached a relatively stable shape and size, and further elutriation was reduced to less than 1% over 20 h. Changes in particle shape during testing are undesirable, not only because of the possible changing particle abrasivity, but also because the associated change in particle size distribution alters the state of fluidization. Accordingly, all tests were carried out with bed material that had been preconditioned in the fluidized bed. Furthermore, the finer bed material that had naturally levitated to the top of the bed during fluidization was vacuumed off and replaced with fresh material between test increments. These procedures yielded bed material that was of a satisfactorily consistent size and shape distribution over a time in excess of 1000 h. A typical collection of conditioned quartz particles used during testing is shown in the scanning electron micrograph in Fig. 2.



Fig. 2. Collection of typical conditioned quartz particles used in fluidized bed wear study.

3.2. Fluidizing behavior

The wear rate was found to be strongly dependent on the excess fluidizing velocity (u_s , defined as $u_s - u_{mf}$). It is therefore important that u_{mf} be determined precisely, and that u_s be set and monitored accurately. The preferred method for determining the onset of fluidization is to monitor the pressure drop across the bed as u_s is increased [6]. The pressure drop increases linearly until u_{mf} is reached; for velocities higher than u_{mf} the pressure drop remains constant. Invariably the superficial velocity at which the mean pressure drop across the bed becomes constant has been found to coincide with the onset of bubbling. This was anticipated since u_{mb} is predicted to equal u_{mf} for the particle size distribution used. There is some hysteresis in that a small reduction in u_s below u_{mf} once bubbling has commenced does not result in its cessation. It was therefore decided that u_{mf} would be defined as the velocity at which bubbling ceased upon lowering u_s from a value above u_{mf} . The measured u_{mf} values agree with those predicted from calculations to within $\pm 10\%$.

It was found that specimen motion within the bed creates pressure waves that cause and control bubble generation at the distributor. This is true even at superficial velocities somewhat below u_{mf} . Within a bubbling bed, the moving specimen will be subjected to differing load conditions from cycle to cycle depending on the local particle density during the 10 - 20 ms travel interval. This results in peak force values that typically have a standard deviation of between 25% and 35%.

3.3. Forces on specimen rods

The forces experienced by the rods during downward motion are basically governed by the local bed density immediately below the rod. Any factor causing an increase in local bed density, such as the reduction of u_s , or the increase in specimen velocity, results in an increased force experienced by the specimen. The proximity of a passing bubble during motion conversely leads to a reduction in peak force. The force experienced by the top half of the rod on the slow return stroke is limited to around 2% of that which the rod bottom experiences on the down stroke. During the downward stroke, the force on the rod increases in a roughly linear manner from zero up to a maximum value near the end of the stroke. The force returns to zero when vertical motion stops. This peak value is the force that was measured and is referred to in the results and discussion. Typical peak force values are between 50 and 200 N. The magnitude of this force and its periodic pulsing nature are similar to that measured in larger experimental fluidized bed rigs [5].

4. Experimental procedure

4.1. Mass loss measurements

All wear testing under a given set of conditions was carried out in a succession of individual increments that ranged in duration from 4 to 65 h.

Incremental testing was necessary because all of the metallic materials exhibited an incubation period during which the initial rate of mass loss was considerably lower than the steady state value. In some instances, a mass gain was recorded during the first increment. The duration of the incubation period varied, but was typically between 20 and 60 h. The specimens were weighed between increments on a balance with a resolution of 0.1 mg. Measured incremental losses were typically in a range 2 - 70 mg. Earlier results indicated that ultrasonic cleaning of the specimen between increments, prior to weighing, altered the steady state surface condition [7]. The specimens were therefore handled carefully between increments and cleaned only with an air jet. Wear rates were determined from the linear regression of the cumulative mass loss *vs.* exposure time in the steady state regime. Linear correlation coefficients *r* are quoted to give an indication of reproducibility and the achievement of steady state.

4.2. Thickness loss measurements

In Task 2, thickness loss measurements were taken in approximately 7.5° intervals around the ^{periphery} ~~periphery~~ of the rods using a diamond stylus profilometer. Measurements were made relative to a small circumferential masked region at the midpoint along the specimen axis. A practical accuracy of 1 μm could usually be guaranteed for small losses. For larger losses, the error was limited to ±5%. The circumferential accuracy was limited to ±2°. Profiles were taken after completion of each incremental series; taking measurements between increments was generally not practical owing to the small losses involved. The profiles obtained were used to determine wear distribution but were not directly used in determining steady state wear rates because the varying incubation behavior of the different materials makes comparisons among them misleading. As will be shown below, losses were generally limited to two reasonably symmetric circumferential regions of between 25° and 35° in width. The quoted thickness loss values were determined by averaging the steady state loss rate, determined from mass loss measurements, over the area encompassed by the circumferential widths of the two loss regions, determined by profilometry. This width was defined as the circumferential width of each loss region at half the maximum peak height. This is shown schematically in Fig. 3. The thickness loss rates determined in this manner were typically between 30% and 50% higher than the peak thickness loss rates determined directly from loss profiles. Much of this difference is due to the inclusion of the incubation periods in the loss rates estimated from the thickness profiles.

4.3. Task 1

The purpose of this task was to investigate the effects of varying both fluidizing velocity and specimen location beneath the bed surface. The results were to aid the selection of an appropriate set of operating conditions for future studies. A 6061-T6 aluminum specimen rod, which was pre-

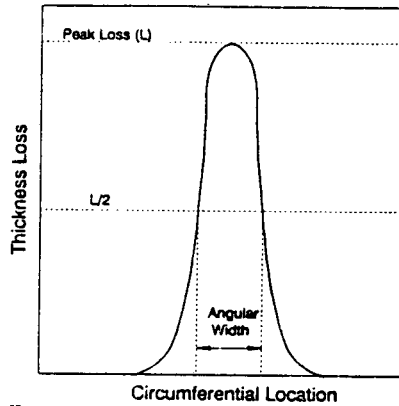


Fig. 3. Schematic of method used to determine the area over which the rod wastage is averaged.

TABLE 2

Test conditions for Tasks 1 and 2

Test conditions	Task 1	Task 2
Bed material	Conditioned SiO ₂	Conditioned SiO ₂
Bed depth	457 or 406 mm	457 mm
Mean particle size	800 μm	750 μm ^a
Rod depth below bed surface	25 or 76 mm	76 mm
Minimum fluidizing velocity	0.42 m s ⁻¹	0.32 to 0.38 m s ⁻¹
State of fluidization (u_x)	0; 0.05; 0.10 m s ⁻¹	0
Actuating pressure	140 kPa	280 kPa
Actuating frequency	1 Hz	1 Hz
Actuation displacement	10 mm	10 mm

^aThe reduction in particle diameter from Task 1 to Task 2 is not significant. It resulted from the particle conditioning procedure not being fully established at the time of the Task 1 tests.

exposed in the rig to eliminate incubation effects due to initial particle embedment, was tested under six sets of operating conditions. The specimen was located either 76 or 25 mm (3 or 1 in.) below the bed surface, and the bed was fluidized to three different excess fluidizing velocities u_x . Incremental tests of varying times, ranging from 4 to 20 h, typically 10 h, were continued for each set of conditions until the linear wear behavior was established. The test conditions are listed in Table 2.

4.4. Task 2

This task was designed as an investigation into the effects of material properties on tube wear. Pure metals and alloys were tested under the same set of conditions. The materials were weighed between increments of varying times ranging from 6 to 65 h but were generally near 20 h. Total exposure

times ranged from 90 to 250 h. Thickness loss profiles were taken at the conclusion of each test. The test conditions are listed alongside those of Task 1 in Table 2. The materials selected for this task are listed in Table 3.

5. Results and discussion

5.1. Task 1

The six steady state loss rates determined from plots of cumulative mass loss as a function of bed exposure time are presented in Table 4 and graphed in Fig. 4(a). Two trends in material wear are clearly evident. First, there is a decrease in the wear rate associated with an increase in excess fluidizing velocity. This is expected since the bed resistance force is greatly reduced with an increase of u_s in the neighborhood of u_{mf} . A second trend is the fractional decrease in wear rate for a specimen situated closer to the bed surface. It is possible that the agglomeration of bursting bubbles close to the bed surface results in a reduced bed density in this region such that on the downward stroke, particles are loaded onto the specimen surface

TABLE 3
Description of materials tested in Task 2

Material	Composition (wt.%)	Heat treatment
Aluminum	99.999	Annealed
Copper	99.9999	Annealed
Nickel	99.99	Annealed
Iron	99.95	Annealed
6061-T6 Aluminum	1.0 Mg, 0.6 Si, 0.3 Cu 0.3 Cr	As supplied aged condition
4140 steel	1.0 Cr, 0.8 Mn, 0.40 C, 0.3 Si, 0.2 Mo	Normalized or oil quenched and tempered at 400 °C, 1 h

TABLE 4
Task 1 wear rates

u_x (m s ⁻¹)	Depth of specimen in bed (mm)	Loss ^a (mg m ⁻² h ⁻¹)	r^b
0	76	200	0.9990
0.05	76	132	0.9992
0.10	76	90	0.9980
0	25	187	0.9992
0.05	25	95	0.9988
0.10	25	58	0.9993

^aLosses averaged over entire rod surface.

^b r , linear correlation coefficient.

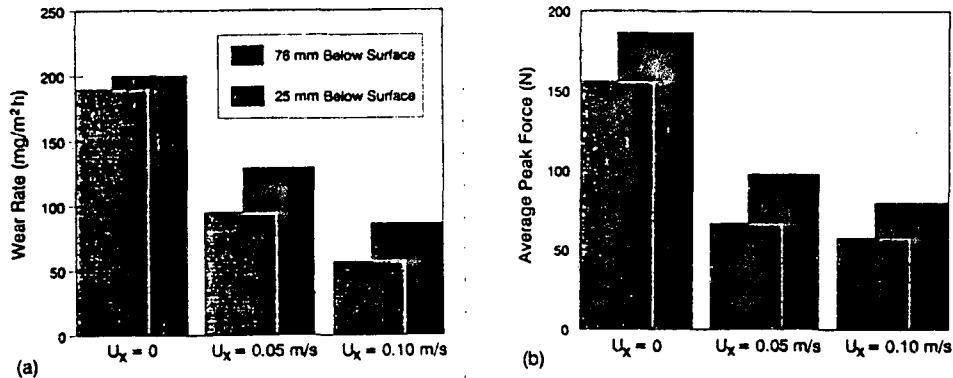


Fig. 4. (a) Task 1 wear rates as a function of excess fluidizing velocity and depth below bed surface. (b) Mean peak force on specimen under the same conditions.

at lower forces than at the deeper location. The relative effect of this would be expected to increase with an increasing u_x ; this is consistent with the results.

Both of these trends are directly related to the force of impact of the bed material on the specimen as shown in Fig. 4(b). The basic dependency of the wear rate on the force, as the excess fluidizing velocity and rod location are changed, is apparent. It is interesting to note that the force changed comparatively little with an increase in u_x from 0.05 to 0.10 m s^{-1} . This is probably due to a lack of defluidization at these higher excess velocities. The bed in these cases acts more like a viscous fluid. At values of u_x nearer 0, force pulses showed sudden sharp increases part way through the stroke. This was probably related to defluidization.

In an effort to gauge the extent to which this rig simulates the wear experienced in an actual bubbling bed, the wear rates from Task 1 and other actuated specimen rig results were compared to those found by Parkinson *et al.* [8] in their cold model study. The conditions of test Runs 3, 5, and 8 from Parkinson's work closely resemble those of the current study. As part of those runs, a number of aluminum alloy (RTZ HE 30) tubes that had been pre-exposed to eliminate incubation effects were exposed in a bed of quartz particles with a mean diameter of 860 μm and fluidized at a velocity of either 1 or 2 m s^{-1} for at least 48 h. In that study, bed pressure pulses of a frequency between 1 and 2 Hz were observed. Table 5 presents the range of surface-averaged rod wear rates from the present study, along with ranges of surface-averaged tube wear rates calculated from the various quoted tube mass losses from Runs 3, 5, and 8 in ref. [8]. The agreement between the results of Parkinson and those of the actuating rig suggest that the test conditions selected in Task 1 are suitable for use as a basis in further studies. Comparisons of circumferential wear distribution, which are discussed later, also support this conclusion. From Task 1, the value $u_x = 0$ was selected because it resulted in higher loss rates, and because defluidization is believed to have occurred. The actuating pressure used as a base in future

TABLE 5

Comparison of actuating unit wear rates with results from other studies

Source	Approx. wear rate range ^b (mg m ⁻² h ⁻¹)
Actuating unit, Task 1	58 - 200
Actuating unit, other results ^a	200 - 450
Run 3 [8]	200 - 1600
Run 5	100 - 350
Run 8	100 - 350

^aThese results are from work similar to that of Task 1 except carried out in a bed 150 mm deep, and at specimen actuating frequencies up to 2 Hz [7].

^bLosses averaged over entire tube surface.

TABLE 6

Task 2 wear rates

Material	Hardness ^a (kg mm ⁻²)	Loss ^b (nm h ⁻¹)	r ^c
Aluminum (99.999%)	16	707	0.9989
Copper (99.9999%)	36	291	0.9999
Nickel (99.99%)	63	125	0.9992
Iron (99.95%)	92	86	0.9990
6061-T6 Aluminum	120	556	0.9989
4140 Steel (normalized)	165	74	0.9995
4140 Steel (tempered)	370	76	0.9994

^aVickers microhardness test.

^bLosses averaged over two angular half widths of significant material removal determined from individual thickness loss profiles.

^cr, linear correlation coefficient.

studies was doubled to 280 kPa for similar reasons. The median depth of the specimen below the bed surface was selected to be 76 mm because the fluidizing environment is more uniform at this deeper location. All other conditions remained unchanged.

5.2. Task 2

5.2.1. Rates of material wear

The wear rates for the various materials tested in Task 2 are listed in Table 6 together with their hardness values. The relationship between the wear resistance (1/wear rate) of the metallic materials tested in Task 2 and their hardness is plotted in Fig. 5. Wear resistance is seen to increase linearly with the annealed hardness of pure metals. This relationship was anticipated and has been shown to exist for two-body abrasion (Khrushchov [9], Richardson [10]), three-body abrasion (Misra and Finnie [11]), and erosion

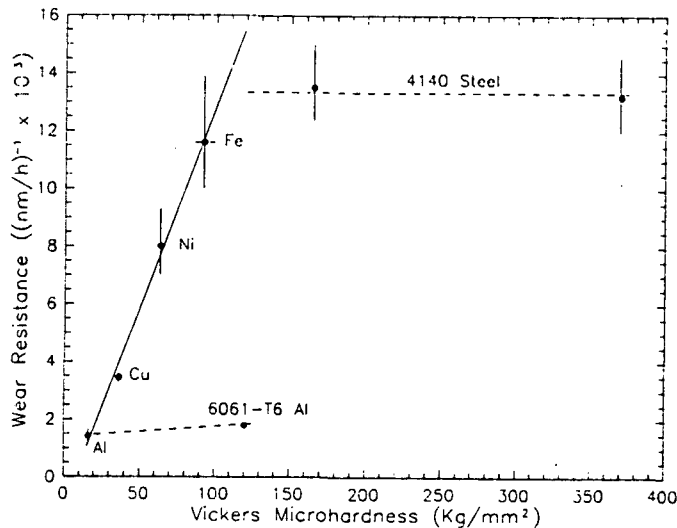


Fig. 5. Wear resistance of Task 2 materials as a function of hardness.

(Finnie *et al.* [12]). It is also indicated in Fig. 5 that increased hardness resulting from precipitation strengthening or heat treatment had comparatively little effect. The thermally hardened 4140 steel showed no improvement in wear resistance over the normalized material. This result was also obtained by Finnie *et al.* for the erosion of 1045 steel [12]. Others have shown a slight increase in wear resistance for similar thermally treated materials tested under abrasive conditions [9 - 11].

5.2.2. Wear distribution and morphology

Figure 6 shows the thickness loss profile for the pure copper specimen. It is characteristic of the profiles for all of the metallic materials with the exception of the pure aluminum. The wear patterns of these more typical specimen rods can be divided into four regions of differing behavior and morphology. The regions (referenced to 0° at the rod top) are as follows.

(1) 0° - 80° (280° - 360°). No thickness loss at all was found on the top half of the rods. Instead, there was a gradual increase in thickness with the maximum occurring at the rod top. This is indicative of a layer of deposited bed material covering the surface. This deposit can be seen in the optical micrograph of the 0° location on the 6061-T6 Al specimen in Fig. 7. Shown in the cross-section is part of the continuous layer that is composed of micron-sized quartz particle fragments held in a conglomerate of submicron quartz. The maximum deposit thickness ranged from 2 to 10 μm for the different materials.

(2) 80° - 100° (260° - 280°). No thickness change was found on the rod sides at 90° and 270°, and there was little surface deformation or particle

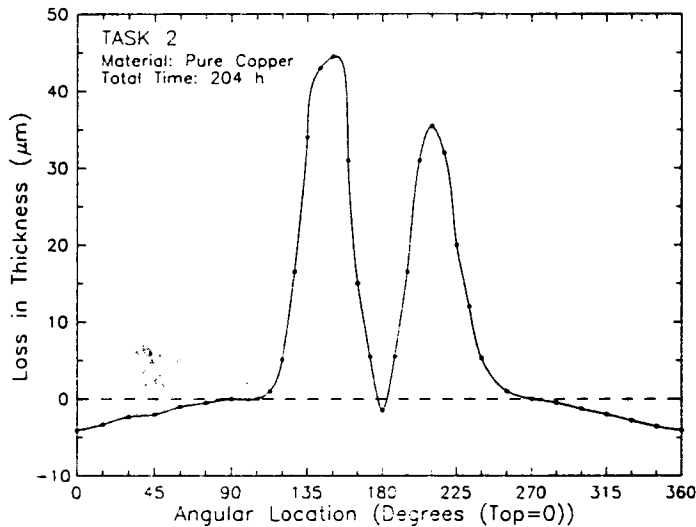


Fig. 6. Circumferential thickness loss profile of Task 2 copper specimen rod at the conclusion of 204 h of testing.



Fig. 7. Optical micrograph of surface cross-section from the 0° rod location of the 6061-T6 specimen from Task 2 showing deposit layer on surface.

embedment. This is expected, since the normal load on particles contacting the surface at this location is at a minimum.

(3) 100° - 170° (190° - 260°). These regions were the only locations on the rod to experience any substantial material removal. Maximum loss consistently occurred at 145 and 215° ± 3°. Examination of the worn 6061-T6 Al rod surface in this region revealed many small abrasion tracks, as seen in Fig. 8(a), as well as indentations of the kind shown in Fig. 8(b). The surface surrounding these abrasion scars was covered with a layer of fine quartz particles, probably similar in make-up to that seen on the rod top, though of a different thickness. The basins of fresh scars usually had no quartz layer, indicating that the impacts could penetrate through the layer to deform or remove underlying metal. The wear tracks typically had widths

215° ± 3°

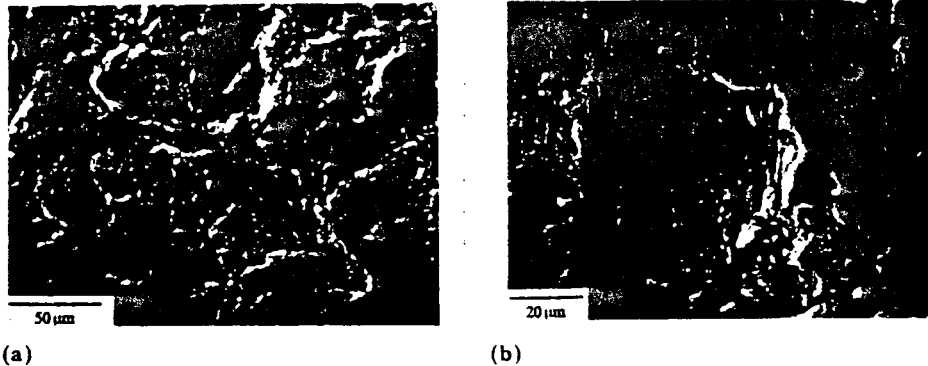


Fig. 8. SEM images of the worn 6061-T6 aluminum surface at the angular rod location of 145° showing: (a) a typical abrasion scar, and (b) an indentation. The tops of the images are closest to the top of the rod.

that were only 4% of the $750 \mu\text{m}$ mean bed particle diameter. Many tracks showed evidence of particle rotation and change in loading or direction during contact with the specimen. This is characteristic of the wear events expected in three-body abrasion.

The abrasion tracks on the 6061-T6 Al were on average $20 \mu\text{m}$ wide, $80 \mu\text{m}$ long, and only $1 \mu\text{m}$ deep. There were very few tracks at the rod bottoms and none were found on the top halves of the rods. From the observed average abrasion scar dimensions, it is estimated that a typical impact might remove $1.60 \times 10^{-6} \text{ mm}^3$. From the 6061-T6 Al thickness loss profile, the total volume lost during the 130 h of the bed exposure was found to be approximately 52 mm^3 distributed over two 30° circumferential regions where significant loss occurred. Thus there might have been 32.5 million impacts during the 130 h. This is equivalent to only 1 impact mm^{-2} per 15 specimen strokes. Each of these impacts results in the cutting of material from the surface and the displacement of material to the sides and front of the scar. If only 20% of the scar volume is removed from the surface, then it would require only 1 impact mm^{-2} per 3 specimen strokes to account for the observed rate of wear. Since the specimen on each stroke moves 10 mm through a densely packed bed of 0.75 mm particles, several impacts per mm^2 would be expected. The observed wear tracks alone can thus easily account for the metal loss even if most of the displaced material was not immediately removed from the surface.

The surface region at the 145° location on the 6061-T6 Al rod is shown in cross-section in Fig. 9. The surface is composed of a layer of mixed quartz and aluminum between 2 and $10 \mu\text{m}$ thick. The mixed layer was particularly thick in the region shown. Its marbled appearance is due to the presence of highly deformed metal foils sandwiched between layers of micron and submicron sized quartz debris. The foils can be seen in the micrograph to be aligned with the direction of particle flow during the

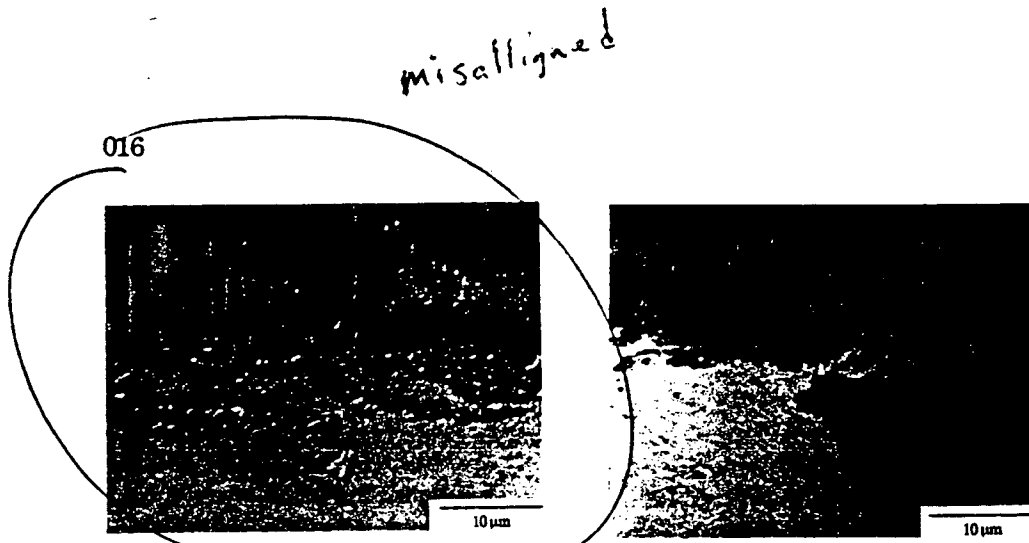


Fig. 9. Optical image of the worn 6061-T6 aluminum surface seen in cross-section near the 145° location. Rod top is towards the left.

Fig. 10. Representative optical image of the worn 6061-T6 aluminum surface seen in cross-section near the 180° location.

downward specimen stroke. The formation of metal foils has also been found in studies of the wasted heat exchanger tubes from the Grimethorpe Pressurized FBC Facility [13]. In that study, metal "slivers" 1 - 3 μm thick were present in the wasted regions at the substrate-deposit interface and were aligned with the flow direction of the bed material. The authors noted a similarity between the observed worn tube microstructure and that resulting from a ball-milling process. It was also suggested that forces necessary to produce such deformation might occur during the impact of wakes of passing bubbles.

The wear morphology of the copper specimen was essentially similar, but at a finer scale, to that of the 6061-T6 Al. The harder metals and steels had similar wear scars, though their surfaces could not be resolved in cross section.

(4) 170° - 190°. Except for the case of the pure aluminum, the rod bottoms experienced no thickness loss. Rather, there was a gain in thickness similar to that which occurred on the top half of the rods. The surface morphology at this location was, however, considerably different from that of the rod top. The rod bottom suffered severe deformation and experienced much embedment. This can be seen for the case of the 6061-T6 Al in the optical micrograph in Fig. 10. Such deformation at this location is not surprising given that the greatest particle impact force is experienced at the bottom center of the advancing rod. What is surprising is that even with this relatively large deformation, no significant loss occurred at this location over the 90 - 200 h of bed exposure. This is probably due to the trapping of abrasive particles against the rod bottom during the early part of the downward stroke. This trapping would prevent particles from sliding along the surface and would thus limit wear at the 180° location.

That such a variety of metals and alloys all have the same wear pattern is an indication that the wear profile might be independent of mechanical properties and rely solely on particle flow and impact characteristics. How-

ever, the results of the pure aluminum tests indicate that under some conditions mechanical properties do play a role. The pure aluminum rod, in contrast to all other metals and alloys tested, suffered a significant amount of wear at the rod bottom as can be seen in the wear profile in Fig. 11. In other respects, the pattern of loss was the same. This differing behavior was not related to test duration or magnitude of loss. A pure aluminum rod showed significant loss at the bottom when the peak loss was only $33\ \mu\text{m}$ and the test duration was 115 h. The 6061-T6 Al rod had a peak loss of $55\ \mu\text{m}$ after 130 h, but suffered no loss at the bottom.

Examination of the aluminum rod surface in cross-section revealed it to be considerably more deformed than the other materials. The intermixed aluminum/quartz layer at the rod bottom was as thick as $40\ \mu\text{m}$. A typical area of this layer is shown in Fig. 12. The multiple alternating quartz and

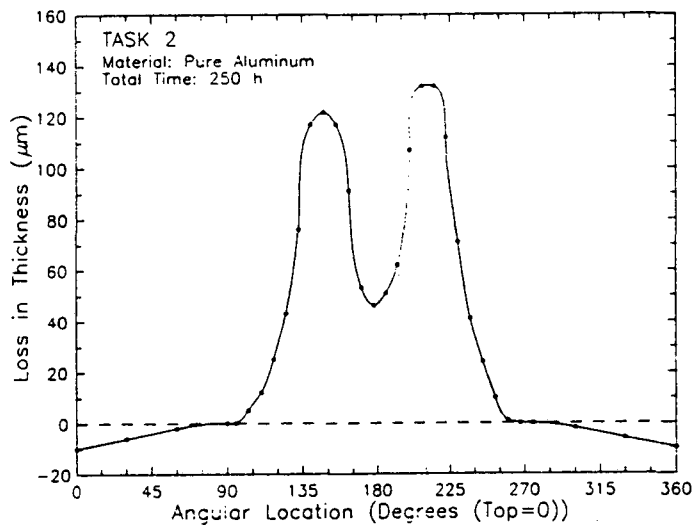


Fig. 11. Circumferential thickness loss profile of pure aluminum specimen rod at the conclusion of 250 h of testing.

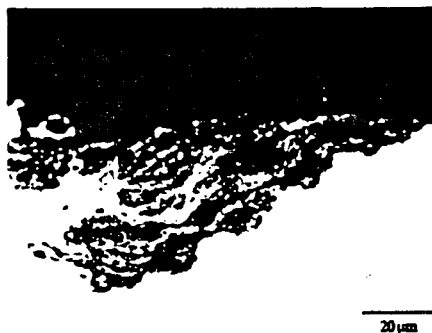


Fig. 12. Representative optical image of the worn pure aluminum surface seen in cross-section near the 180° location.

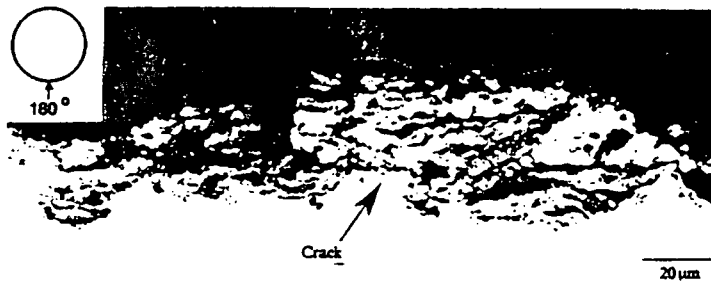


Fig. 13. Optical image of the worn pure aluminum surface seen in cross section near the 180° location showing evidence of failure due to layer cracking.

aluminum layers should be noted. Vickers microhardness measurements revealed this composite layer to be approximately five times harder than the underlying pure aluminum. Many cracks were observed within the layer; in Fig. 13, a crack is seen that has severed a 25 μm thick segment from the surface. Some of the observed cracking was undoubtedly initiated by the metallographic preparation, but many examples were found that indicated segments had spalled prior to specimen preparation. The very low yield stress and high elongation of the pure aluminum allowed the very thick composite to develop with up to 18 or so alternating quartz and aluminum layers. The intermixed region of the pure copper by contrast, was limited to around six component layers and a total thickness of 10 μm . The pure aluminum was probably able to develop a thick enough layer such that the external and internal stresses caused spalling of segments. This layer cracking and spallation may be the sole cause of material removal near the rod bottom and it is likely to have contributed to the loss in the 145° regions as well.

The wear patterns of the rods exposed in this rig are similar to those found in other cold model studies. Parkinson *et al.* [8] using tubes coated with paint layers determined that the maximum wear rate occurred at 36° to either side of the tube bottom (144° and 216°). Subsequent work by Parkinson *et al.* on PVC tubes has supported these findings [14]. This is in agreement with the results from the experimental rig reported here (145° and 215° \pm 3°). The primary difference between these results was that the tubes of Parkinson showed significant loss at the 180° location. This may be related to the difference in mechanical properties between paint and PVC, as compared with metals and alloys. It may also be due to the presence of lateral bed particle motion in the typical fluidized bed unit. The collapse of real bubbles or teardrop voids against the tube surface is rarely symmetric and would therefore result in a net particle flow along the tube surface at the 180° location.

6. Conclusions

The actuated specimen fluidized bed testing rig produced metal wastages similar in rate, distribution, and appearance to those found in other

fluidized bed studies. This suggests that the particle block impact process plays an important role in determining the overall wastage of horizontal heat exchanger tubes in bubbling fbc. Other results were as follows.

(1) Wear rates were found to be directly related to the force of the defluidized particles impacting the specimen.

(2) The relationships between wear resistance and hardness of pure annealed metals and heat treated alloys as reported in the literature were also found in the fluidized bed environment of the testing rig.

(3) Alloys and pure metals (with the exception of pure aluminum) ranging from 36 to 370 Vickers hardness all showed the same wear distribution around the periphery of the specimen rod. No wear occurred on the top half of the rod or at the very bottom. Maximum wear occurred at the 145° and 215° location.

(4) The principal mechanism of material removal appears to be one of three-body microabrasion of a surface layer consisting of a deformation induced mixture of quartz bed material and base metal.

(5) The pure aluminum experienced significant loss on the rod bottom owing to the development and subsequent spalling of a thick intermixed quartz and aluminum layer. Other than this, the wear distribution was the same as that of the other metallic materials tested.

Acknowledgment

This work is being supported by the Electric Power Research Institute under Research Project RP8000-6, through USDOE contract DE-AC03-76 SF00098. ✓

References

- 1 J. Stringer, Current information on metal wastage in fluidized bed combustors. *Proc. 9th Int. Conf. on Fluidized Bed Combustion, Boston, MA, May, 1987, Vol. 2, p. 685.*
- 2 J. Stringer and I. G. Wright, Erosion/corrosion in FBC boilers. *Proc. EPRI Workshop on Wastage of In-Bed Surfaces in Fluidized-Bed Combustors, Argonne, IL, November 2 - 6, 1987.*
- 3 S. A. Jansson, Videotape shown to EPRI workshop on FBC materials issues, Port Hawkesbury, Nova Scotia, August, 1985.
- 4 M. J. Parkinson, Work conducted at British Coal/Coal Research Establishment, Stoke Orchard, U.K.
- 5 T. C. Kennedy, A study of forces on immersed tubes in fluidized beds, *EPRI CS-1542, Project 718-2, Topical Rep.*, 1980.
- 6 J. R. Grace, Fluidized-bed hydrodynamics. In G. Hetsroni (ed.), *Handbook of Multi-phase Systems*, McGraw-Hill, New York, 1981, Chapter 8.
- 7 S. MacAdam and J. Stringer, Development of an actuated specimen fluidized bed wear testing unit. *Proc. EPRI Workshop on Wastage of In-Bed Surfaces in Fluidized-Bed Combustors, November 2 - 6, 1987, Argonne.*
- 8 M. J. Parkinson, J. F. G. Grainger, A. W. Jury and T. J. Kempton, Tube erosion at IEA Grimethorpe: cold model studies at CRE, Tube Bank C, *Metal Wastage Status*

①
 Same source as Ref. 2. Proceeding were distributed in photocopy form and were not published. The paper was 5.8. Ref. 2 has a paper * of 1.1.

- Rep., NCB, IEA Grimethore, Ltd., August, 1983, DOE/ET/10393-1623, January, 1984.
- 9 M. M. Khrushchov, The correlation between wear resistance in abrasive wear and the strength properties of metals, *Ind. Lab.*, 28 (1962) 372 - 376 (translation).
 - 10 R. C. D. Richardson, The maximum hardness of strained surfaces and the abrasive wear of metals and alloys, *Wear*, 10 (1967) 338.
 - 11 A. Misra and I. Finnie, An experimental study of three-body abrasive wear, *Wear*, 85 (1983) 57.
 - 12 I. Finnie, J. Wolak and Y. H. Kabil, Erosion of metals by solid particles, *J. Mater.*, 2 (1967) 682.
 - 13 C. E. Witherall and R. G. Meisenheimer, Tubing wastage in fluidized-bed coal combustors, Test Series 2 NCB, IEA Grimethorpe, Ltd., UCRL-21039, S/C AA-35-10-10-0, January, 1988, Lawrence Livermore National Laboratory, Livermore, CA.
 - 14 M. J. Parkinson, B. A. Napier, A. W. Jury and T. J. Kempton, Cold model studies of PFBC erosion, *Proc. EPRI Workshop on Materials Issues in Fluidized Bed Combustion, Nova Scotia, July, 1985*, Paper No. 15.

LAWRENCE BERKELEY LABORATORY
TECHNICAL INFORMATION DEPARTMENT
1 CYCLOTRON ROAD
BERKELEY, CALIFORNIA 94720